Highlights

Integrated modelling of insect population dynamics at two temporal scales

Emily B. Dennis, Marc Kéry, Byron J.T. Morgan, Armin Coray, Michael Schaub, Bruno Baur

- We model population decline of the endangered beetle *Iberodorcadion fuliginator*.
- Population size is modelled at two temporal scales for a two-year life cycle.
- Integrated population modelling enables true abundance estimation.
- The models include productivity, phenology, survival and detection parameters.
- Our model can improve ecological understanding for rare species with limited data.

Integrated modelling of insect population dynamics at two temporal scales

Emily B. Dennis[a,b,*], Marc Kéry[c], Byron J.T. Morgan[a], Armin Coray[d], Michael Schaub[c], Bruno Baur[e]

[a]*School of Mathematics, Statistics and Actuarial Science, University of Kent, Canterbury, Kent, U.K.*
[b]*Butterfly Conservation, Manor Yard, East Lulworth, Wareham, Dorset, U.K.*
[c]*Swiss Ornithological Institute, Sempach, Switzerland*
[d]*Natural History Museum, Augustinergasse 2, CH-4001 Basel, Switzerland*
[e]*Section of Conservation Biology, Department of Environmental Sciences, University of Basel, St. Johanns-Vorstadt 10, CH-4056 Basel, Switzerland*

Abstract

Population size of species with birth-pulse life-cycles varies both within and between seasons, but most population dynamics models assume that a population can be characterised adequately by a single number within a season. However, within-season dynamics can sometimes be too substantial to be ignored when modelling dynamics between seasons. Typical examples are insect populations or migratory animals. Numerous models for only between-season dynamics exist, but very few have combined dynamics at both temporal scales.

In a new approach, we extend appreciably the models of Dennis et al (2016b): we show how to adapt them for a generation time >1 year and fit an integrated population model for multiple data types, by maximising a joint likelihood for population counts of unmarked individuals and capture-recapture data from a study with marked individuals. We illustrate the approach using annual monitoring data for the endangered flightless beetle *Iberodorcadion fuliginator* from 18 populations in the Upper Rhine Valley for 1998–2016, with a 2-year life cycle. Standard likelihood methods are used for model fitting and comparison, and a concentrated (profile) likelihood approach provides computational efficiency.

Additional information from the capture-recapture data makes the population model more robust and, importantly, enables true, rather than relative, abundance to be estimated. A dynamic stopover model provides estimates of both survival and phenology parameters within a season, and also of productivity between seasons. For *I. fuliginator*, we demonstrate

*Corresponding author
Email address: edennis@butterfly-conservation.org (Emily B. Dennis)

a population decline since 1998 and how this links with productivity, which is affected by temperature. A delayed mean emergence date in recent years is also shown.

A main point of interest is the focus on the two temporal scales at which perhaps most animal populations vary: in the short-term, a population is seldom truly closed within a single season, and in the long term (between seasons) it never is. Hence our models may serve as a template for a general description of population dynamics in many species. This includes rare species with limited data sets, for which there is a general lack of population dynamic models, yet conservation actions may greatly benefit from this kind of models.

Keywords: Beetle, Endangered, *Iberodorcadion fuliginator*, integrated population model, Multi-scale population dynamics, Population model

---

1. Introduction

Most models of population dynamics assume a study species with a birth-pulse life-cycle in a seasonal environment, i.e., a species that reproduces during a particular time of the year, typically in the spring or summer in temperate or cold latitudes. A discrete-time model with autoregressive representation of population dynamics is then typically chosen, where the state of a population at time $t + 1$ is expressed as a function of its state at time t, including parameters that describe the state transition rates between seasons, e.g., demographic or growth rate parameters. Especially for large animals, such as most birds and mammals, it is assumed that the state (typically abundance N, which may be stratified by age or other classification factors), can be characterised by a single number (or a vector of such numbers) at time t. Matrix projection models are the typical example of such models (Caswell, 2001) and have proved to be extremely powerful for modelling population dynamics between seasons. Moreover, N may be estimated using adequate data such that imperfect detection can be accounted for, e.g. distance or capture-recapture sampling (McCrea and Morgan, 2014; Buckland et al., 2015; Böhning et al., 2017). The literature on population dynamics across seasons is extensive (e.g. Koons et al., 2017).

However, many situations exist where the abundance of a population at time t cannot easily be characterised because the population is open within a season and there may be

a constant flux of individuals through the area defining a population. An estimate of N then comprises all individuals that enter and leave the area within a season. Examples are provided by migratory animals at stopover sites, reptiles and pond-breeding amphibians (Matechou et al., 2016), or conceivably migratory wildlife at any observation point (e.g., whales or salmon along a stretch of shore or river, respectively): abundance within a season is then governed by the rates at which new animals arrive, stay and eventually depart again. Another example, which provides the motivation for the present paper, is provided by the imago stage of insects, many of which exhibit typical "phenological curves" within a season. The modelling of population dynamics for species with such pronounced short-term dynamics presents a challenge, because the changes in numbers must be described at two temporal scales: not only between seasons but also within each season.

Previous population dynamics modelling within seasons involves stopover models (e.g. Schaub et al., 2001; Matechou et al., 2014) and phenological curves. The seminal Manly-Zonneveld (MZ) model describes numbers within a season as a function of abundance, mean and spread of emergence date, and a constant survival probability (Manly, 1974; Zonneveld, 1991). This model was generalised to species with multiple generations within a season by Matechou et al. (2014) and Dennis et al. (2016b, henceforth DMFRB). Both approaches describe the trajectory of an observable population from zero to some maximum and back to zero again within one season. In stopover models, gains and losses for the population of staging animals are represented predominantly by arrival and departure, while for one insect generation, they are mostly represented by rates of birth/emergence and death.

DMFRB developed a multi-scale population dynamics model for univoltine and bivoltine butterfly species (i.e., with generation time < 1 year). We extend their model in two important ways: we adapt the model to a biennial life-cycle, where annual cohorts are essentially demographically closed and there are distinct generations from odd and even years, and we fit multi-scale population dynamics models as an integrated population model (IPM; Besbeas et al., 2002; Schaub and Abadi, 2011) by jointly fitting them to two data types: a multivariate time-series of counts of unmarked individuals and a capture-recapture data set

from marked animals.

Our motivating example is an ongoing, long-term population study on the endangered, flightless beetle *Iberodorcadion fuliginator* at the Southern end of the Upper Rhine valley. As well as being important in itself for an improved understanding for this conservation flagship species, the analyses of this data set illustrate how to meet the challenges of modelling long time series of data on rare species and result in definite conclusions.

2. Material and Methods

2.1. Study species and area

The beetle *I. fuliginator* has a life cycle of 2 years (Baur et al., 1997). Females deposit their eggs in stems of grass, preferably *Bromus erectus*, their main larval host plant, in late March through to May. The larvae hatch in May or June, feed on grass roots and pupate after c.14 months (including one hibernation in a late larval stage). Imagos (14–17 mm body length) eclose after 2–3 weeks in July or August, but rest in the soil until the end of the second hibernation. Depending on weather conditions, imagos emerge from the soil in March or April and are sexually active for c.1 month before they die.

Beetle populations were studied near the Swiss city of Basel (47.56°N, 7.58°E), in France, Germany and Switzerland. The maximum extent of the study area defined by the locations of the populations is about 16 km in North-South and about 12 km in East-West directions. See Baur et al. (1997, 2002, 2005) and Table S1 in the Supporting Information for features of the study populations. We use 'site' and 'population' synonymously.

2.2. Field methods

We use data from three field studies: (1) repeated counts of adult beetles in 18 populations from 19 years, (2) intensive, single-year capture-recapture studies in three of these populations, and (3) soil temperature measured over 16 years in Birsfelden, Switzerland (B. Baur, unpublished). Data associated with this analysis can be found here `https://doi.org/10.6084/m9.figshare.7740254.v1`.

2.2.1. Population counts

After the 1990s, 18 populations were found in the study area (see Baur et al. 2002), and are summarised in Table S1 of the Supporting Information. For two populations (Basel and Allschwil) count data were available from 1998 and for the remainder only from 2001 onwards (up to 2016). Populations were surveyed repeatedly during each activity period of *I. fuliginator* (March-May), with typically 4–8 intensive surveys each lasting for up to several hours and sometimes involving several people. In most populations, total search time was 240 minutes per year and survey durations took an average of 40 minutes (range 1–260 minutes).

2.2.2. Capture-recapture study

Data from intensive capture-recapture studies were available from three sites in two different years (Baur et al., 2005). In total 345 beetles were marked uniquely using coloured nail varnish, and recaptured during 20 daily occasions at site Basel (1st April - 22nd May 1988). Between 19th April and 7th June 2000, 433 beetles were marked/recaptured at site Istein during 27 days and 102 beetles at site Huttingen during 21 days. On each day the study sites were carefully searched for *I. fuliginator* for several hours and survey duration (person-hours) was recorded as a measure of effort. Survey durations ranged from 1.7–8.3 hours (mean 6.1) in Basel, from 3.0–16.0 hours (mean 9.5) in Istein and from 3.5–9.3 hours (mean 6.5) in Huttingen. Capture-recapture proceeded as described in Baur et al. (2005). Note that throughout we estimate apparent survival, due to possible movement of beetles outside survey areas.

2.2.3. Temperature covariates: Heat load at each site, and sum of effective temperatures (SET)

The development time of *I. fuliginator* depends on soil temperature, which can be expressed as the sum of effective temperatures (SET), which is the sum of the temperature above the lower developmental threshold (LDT), the temperature below which there is no development.

We use measures of between-site (equivalent to between-population) and between-year variation in soil temperature. As a proxy for between-site differences in mean soil temperature, we calculated the mean heat load (HL) for each site using the model of McCune and Keon (2002), which incorporates topographical variables (aspect, inclination) and latitude.

For between-year variation in soil temperature, we used soil temperature measurements at a depth of 5 cm, which corresponds to the depth at which the larvae live, in a patch of nutrient-poor grassland in Birsfelden, about 5 km from the nearest population in our study (Basel). Soil temperature was recorded at intervals of 3 h over 16 years (2001–2016) using Tinytalk temperature loggers (GeminiData Loggers, Chichester, UK). In the analyses, we used mean soil temperature per day obtained from six measurements. In model fitting we use degree-days (DD; one value for each year, taking the same value for all sites) as a measure of cumulative soil temperature - these are the summation of temperature differences over time, which capture both extremity and duration of higher temperatures. However, for *I. fuliginator* the LDT is unknown, hence we calculated DD for 11 different LDT values (7–17 °C) and each time fitted our model to then determine which LDT value provides the best explanation of the observed data, in terms of predictive power, using Akaike's information criterion (AIC) - see Section 2.8.

We also use the daily mean temperature at Basel (TEMP) from 1998 to 2016 to describe detection probability (M. Baumann, Meteorological Office of Basel, Switzerland).

2.3. The dynamic model and productivity parameters

We extend a dynamic model which was originally designed for butterflies (DMFRB). We denote the counts by $\{y_{i,j,k}\}$, taken on site i, during visit j, and year k, assuming that data are collected for S sites, each visited on $\leq T$ occasions, across K successive years. Each count can be treated as the realisation of an independent random variable from a Poisson distribution with expectation $\lambda_{i,j,k}$. We assume independence since the counts were taken far apart in time and space. The likelihood then has the form

$$\mathrm{L}_S(\boldsymbol{\rho}, \boldsymbol{a}, \boldsymbol{p}, \boldsymbol{N}; \boldsymbol{y}) = \prod_{i=1}^{S} \prod_{j=1}^{T} \prod_{k=1}^{K} \frac{\exp(-\lambda_{i,j,k}) \lambda_{i,j,k}^{y_{i,j,k}}}{y_{i,j,k}!}. \quad (1)$$

We use boldface to indicate vectors and matrices, and we describe the model parameters below. For a general model we let

$$\lambda_{i,j,k} = N_{i,k} p_{i,j,k} a_{i,j,k}, \tag{2}$$

where

- $N_{i,k}$ denotes abundance (= number of individuals ever alive) at site i in year k,
- $p_{i,j,k}$ is the detection probability for visit j, at site i in year k,
- $a_{i,j,k}$ is a unimodal function that describes the within-season variation of abundance.

Equation 2 contains detection probabilities, which did not feature in the models of DMFRB. In principle such parameters can be estimated from count data alone, making use of covariate regressions (Matechou et al., 2014). However this can be difficult in practice, due to the limited amount of information (Knape and Korner 2015). Thus we only introduce detection probabilities when an integrated analysis is performed; where the model is applied to count data alone detection probabilities are not identifiable and are subsumed into $\{N_{i,k}\}$, which is therefore a measure of relative abundance, i.e., the product of N and p, as in DMFRB.

The framework of the DMFRB model allows two approaches for describing within-season variation in abundance: a phenomenological approach, which fits one or more Gaussian curves directly, or a mechanistic stopover approach which fits a birth/death population model and explicitly models the pattern of emergence using one or more Gaussian curves. Here we focus on a mechanistic approach. These models provide alternative forms for the $\{a_{i,j,k}\}$ of Equation 2. Inserting the expression of Equation 2 into Equation 1 provides the likelihood for the survey data, L_S, with additional parameters, $\boldsymbol{\rho}$ and those of $\mathbf{a}$, to be described below. Results, not shown here, from adopting the alternative, phenomenological models (see DMFRB) for our data set are in good agreement with those that we present.

To account for a two-year life cycle we let

$$N_{i,k} = \rho_{i,k-2} N_{i,k-2}. \tag{3}$$

Here, the abundance in a given year depends on the product of the abundance from two years previously and the productivity across the two intermediate years, which is described by the single parameter $\rho_{i,k-2}$. Hence from Equation 2,

$$\lambda_{i,j,1} = N_{i,1} p_{i,j,1} a_{i,j,1}$$

and

$$\lambda_{i,j,2} = N_{i,2} p_{i,j,2} a_{i,j,2},$$

and for $k > 2$, by iterating the relationships of Equation 3, we obtain for Equation 2

$$\lambda_{i,j,k} = N_{i,k} p_{i,j,k} a_{i,j,k} = \begin{cases} \left(N_{i,1} \prod_{m=1}^{(k-1)/2} \rho_{i,2m-1} \right) p_{i,j,k} a_{i,j,k} & \text{if year } k \text{ is odd,} \\ \left(N_{i,2} \prod_{m=1}^{(k-2)/2} \rho_{i,2m} \right) p_{i,j,k} a_{i,j,k} & \text{if year } k \text{ is even.} \end{cases} \tag{4}$$

Equation 3 expresses a simple deterministic relationship and the corresponding stochastic formulation could be modelled in terms of a hidden Markov model (Besbeas and Morgan, 2020). We have investigated both types of model, and found little difference in their results when applied to monitoring data for butterflies in models such as in DMFRB, and so we adopt the simpler model here.

We use the total of the estimates, $\hat{N}_{i,k}$, of the site parameters, $N_{i,k}$, as a measure of overall abundance, $G_k = \sum_i \hat{N}_{i,k}$, for each year k.

2.4. Describing seasonality using a stopover model

We specify $\{a_{i,j,k}\}$ using a stopover model, which builds survival into the models by introducing additional parameters, including the mean emergence times of adults. These phenological parameters are typically unknown, and of interest in their own right as descriptors of a specific, key point in a species' life-cycle and thus potentially useful indicators of phenological change. The approach is based upon the stopover model of Matechou et al. (2014), which DMFRB extended to the analysis of data from multiple years, introducing and estimating productivity parameters.

The expected number of individuals counted at site i at time $t_{i,j,k}$ in year k is given as

$$\lambda_{i,j,k} = N_{i,k} p_{i,j,k} a_{i,j,k} = N_{i,k} p_{i,j,k} \left\{ \sum_{d=1}^{j} \beta_{i,d-1,k} \left(\prod_{m=d}^{j-1} \phi_{i,m,k} \right) \right\}, \tag{5}$$

where the index $d = 1, \ldots, j$, indicates the possible times of emergence for an individual detected on visit j. We define $\phi_{i,m,k}$ as the probability that an individual that is present at site i at visit m in year k will remain at that site until visit $m+1$. The $\beta_{i,d-1,k}$ describe the proportions of $N_{i,k}$ emerging at site i and visit d in year k, such that $\sum_{d=1}^{T} \beta_{i,d-1,k} = 1$, for each site i and year k. In order that this emergence pattern has the right shape for univoltine data, we set

$$\beta_{i,d-1,k} = F_{i,k}(t_{i,d,k}) - F_{i,k}(t_{i,d-1,k}), \tag{6}$$

where $F_{i,k}(t_{i,d,k}) = P(X \leq t_{i,d,k})$ for $X \sim N(\mu_{i,k}, \sigma^2_{i,k})$, $\mu_{i,k}$ is the mean date of emergence and $\sigma^2_{i,k}$ is the associated variance, which represents the spread of the emergence period. Thus the β's are appropriate areas under a Gaussian curve, which ensures that they have the correct shape, starting small, rising to a maximum over time and then reducing to zero as time increases within a season. For each i and k, $\beta_{i,0,k} = F_{i,k}(1)$ and $\beta_{i,T-1,k} = 1 - F_{i,k}(T-1)$.

2.5. Obtaining maximum likelihood parameter estimates by concentrated likelihood

We obtain maximum likelihood parameter estimates for these models via a concentrated (profile) likelihood approach (see DMFRB). The approach reduces the dimensions of the likelihood by optimising with respect to parameters relating only to $\boldsymbol{\rho}$ and $\mathbf{a}$, providing computational efficiency.

We set out to maximise the likelihood of Equation 1 by first forming its first-order derivatives with respect to the individual parameters. When that is done, and the resulting equations are all set equal to zero in search of a maximum, we find that the initial site parameters can be written as a function of the data and other parameters, as

$$N_{i,1} = \sum_{j=1}^{T} \frac{\sum_{k=1}^{(V-1)/2} y_{i,j,2m-1}}{a_{i,j,1} + \sum_{k=1}^{(V-1)/2} a_{i,j,2k+1} \prod_{m=1}^{k} \rho_{i,2m-1}}, \tag{7}$$

and

$$N_{i,2} = \sum_{j=1}^{T} \frac{\sum_{k=1}^{(V-2)/2} y_{i,j,2k}}{a_{i,j,2} + \sum_{k=1}^{(V-2)/2} a_{i,j,2k} \prod_{m=1}^{k} \rho_{i,2m}}. \tag{8}$$

Substituting the expressions of (7) and (8) into the likelihood, we can optimise with respect to parameters relating only to $\boldsymbol{\rho}$ and $\mathbf{a}$.

After the model is fitted, estimates of $\{N_{i,1}\}$ and $\{N_{i,2}\}$ can be obtained by inserting $\hat{\boldsymbol{\rho}}$ and $\hat{\mathbf{a}}$ in Equations 7 and 8, and $\{N_{i,k}\}$ for $k > 2$ are derived from Equation 4. This approach appreciably speeds up the likelihood optimisation. The performance of the dynamic model, adapted to account for a biennial life-cycle, was checked and verified using simulated data (results not shown here). This demonstrates the generality of the concentrated likelihood approach and its potential to be used for taxa with several years in different states.

The likelihood is maximised using the `optim` numerical optimisation function in `R` (R Core Team, 2018). Standard errors were obtained from the inverse of the Hessian matrix at the likelihood maxima, and transformed using the Delta method (Morgan, 2009, p.123), where appropriate link functions were used.

2.6. Capture-recapture modelling

Parameter estimates for apparent daily survival, ϕ, and detection probability, p, were obtained from the capture-recapture (CR) data for the Cormack-Jolly-Seber model (see McCrea and Morgan 2014, p.70), using the `marked` package in `R` (Laake et al., 2013). Separate likelihoods were formed and maximised for the data from each of the three sites. We estimate ϕ as time-independent throughout, and take p to vary logistically with survey duration. We note that Baur et al. (2005) used a Jolly-Seber model to estimate survival using the same data, and also estimate population size for the years 1988 and 2000, for particular sites. The component likelihood, L_M, is given by McCrea and Morgan (2014, p.70).

2.7. Integrated population modelling

Integrated population modelling was initially proposed in the area of fisheries science (see McCrea and Morgan, 2014, p.227). The approach of this paper was proposed by Besbeas et al. (2002). By modelling independent time-series of counts and capture-recapture data through a joint likelihood, which is the product of likelihoods for each component data set, we are able to combine data from different sources on different aspects of the same species

in a single analysis. Common model parameters are thereby estimated more precisely than would otherwise be the case, and a single analysis replaces piecemeal, separate analyses. In general terms, this improves the understanding of the species' ecology. In particular, as we shall see, it may be possible through an integrated analysis to estimate model parameter(s) that would not have been otherwise possible due to confounding. The approach of IPM is now widely adopted, and the area remains one of active research; see for example, Matechou et al. (2013), Besbeas and Morgan (2019) and Schaub and Kéry (2021).

We assume that the capture-recapture and count data sets are independent. Consequently, for IPM likelihoods are formed for the separate data sets, and then multiplied together to form a single joint likelihood, which is maximised to obtain maximum-likelihood estimates of all model parameters that are informed from both the count and CR data simultaneously. The capture-recapture modelling directly informs probabilities of daily survival and detection, which improves estimation of survival in the model for the count data. Moreover, the IPM formulation enables us to estimate absolute, rather than relative abundance.

The concentrated-likelihood approach is also used for the joint likelihood, L_J. Here we have three capture-recapture likelihoods and one count likelihood, and the joint likelihood has the form

$$\mathrm{L}_J = \mathrm{L}_{M_1}\mathrm{L}_{M_2}\mathrm{L}_{M_3}\mathrm{L}_S,$$

where L_S is given in Equation 1 and L_{M_i} is the likelihood for the i^{th} capture-recapture data set. The first three components are functions of ϕ and p parameters only, while the last is a function of all the model parameters. Because the capture-recapture likelihoods were obtained using the `marked` package in `R`, it is convenient to adopt the approach of Besbeas et al. (2003) to construct an approximate likelihood in each case, using a multivariate normal approximation with ϕ and p parameters that are common for the data sets. Each approximate likelihood was based upon the maximum-likelihood estimates from Table S2 in the Supporting Information, and associated estimates of variance and covariance obtained from the inverse Hessian matrix at the likelihood maxima.

2.8. Model selection

We fitted and compared a fairly large number of models to test biological hypotheses about the beetle and to identify model structure that 'best' describes its population dynamics. Following preliminary analysis of the count and capture-recapture data separately (see Supporting Information), we apply the integrated modelling approach, firstly with year-dependent productivity, ρ, either constant or year-dependent mean emergence date μ, with detection probability, p, varying with survey duration (DUR) and all other parameters kept constant.

Prior to performing model selection for additional covariates, an optimal lower developmental threshold (LDT for *I. fuliginator* was chosen as follows. The integrated model was fitted with productivity, ρ, varying only with degree days (DD) for multiple values of LDT (see Section 2.2.3), and the optimal LDT chosen based on the model with lowest AIC. For this purpose both μ and σ were considered constant, and detection probability p varied with survey duration.

The incorporation of additional covariates (including degree-days, DD, with optimal LDT now estimated), to describe productivity and detection probability was then explored, by fitting all model combinations and comparison via AIC. For computational efficiency, model selection was applied to models with constant rather than year-dependent mean emergence date, μ. Productivity, ρ, was modelled as a logistic function of site heat load (HL) and/or DD, as well as year effects (YEAR). For detection probability, p, survey duration (DUR) and temperature (TEMP) were considered, as well as quadratic effects for temperature, again on the logistic scale. Here temperature was the daily mean temperature in Basel (described in Section 2.2.3). Throughout we assume the spread of emergence date, σ, to be constant across site and year, since models with year-variation in both σ and μ will have many parameters to estimate, which is likely to be very time consuming and potentially problematic to fit. Following model selection, the top model was refitted but with year-dependent mean emergence date, μ.

3. Results

3.1. Integrated modelling

We first fit two integrated models to the count and capture-recapture data that assume either a constant or a year-varying mean emergence date μ, but both assume spread of emergence σ and apparent survival ϕ to be constant, detection parameter p to vary with survey duration in a linear-logistic manner, and productivity ρ to be year-varying (Table 1, a and b). Comparison with estimates from the analysis of count data alone (Table 2) shows increased precision from the integrated modelling, as expected. The model with year-varying μ produces an appreciably lower AIC, although there was minimal effect on the other model parameter estimates, except for σ. Estimates of productivity ρ and mean emergence date μ for each year from model b) are shown in Figures S2 and S3 of the Supporting Information and of the population size measure, G, from various integrated models in Figure S4 of the Supporting Information.

Peak emergence date, μ, was estimated later under the integrated model than from the analysis of the count data alone, but estimates of σ were similar, and both parameters were estimated with increased precision (comparing Tables 1a and 2). The integrated models also produce a lower estimate for ϕ, compared with the estimates in Table 2, which we attribute to the role played by detection probability p in the integrated analysis, and its dependence upon survey duration.

Standard errors for all model parameters were at least halved in the integrated analysis, compared to a simpler model for the count data alone, illustrating one of the benefits of this modelling approach.

3.2. Incorporation of additional covariates

Models without the year effect for productivity were fitted first, to compare 11 threshold values for the degree-days covariate. A threshold of 15 degrees C was chosen by AIC, so this value was used in the full model comparison, which included the models where productivity can vary with year as well as degree-days. Although differences in AIC thresholds between

Table 1: Parameter estimates and associated standard errors (SE) for four integrated models, where n denotes the number of parameters estimated for each model. In all models, survival ϕ and the spread of the emergence period σ are constant, and detection probability p varies logistically with survey duration, where p_{int} and p_{DUR} are the intercept and slope parameters, and $\bar{p}$ is the mean estimate of p across durations. In models (a) and (b) productivity ρ varies only with year, whereas in models (c) and (d), following model selection (see Table 3), ρ varies with year and site heat load, where ρ_{HL} represents the slope parameter. Mean emergence date μ is constant in models (a) and (c), but year-dependent in models (b) and (d). Year-dependent parameter estimates (for ρ and μ) are not given but are displayed in plots for selected models.

	a)		b)		c)		d)	
n	22		40		23		41	
AIC	5211.0		5024.3		5183.4		4984.9	
Parameter	Estimate	SE	Estimate	SE	Estimate	SE	Estimate	SE
ρ_{HL}					1.0794	0.1980	1.2902	0.2037
μ	79.0181	3.5847	year-varying		77.7021	3.3293	year-varying	
σ	33.9607	3.1798	22.4269	1.6104	32.7917	3.0024	22.5838	1.6480
ϕ	0.8793	0.0088	0.8757	0.0089	0.8787	0.0088	0.8778	0.0089
p_{int}	-3.0601	0.1567	-3.0628	0.1575	-3.0019	0.1566	-3.0073	0.1565
p_{DUR}	0.1062	0.0167	0.1082	0.0167	0.0996	0.0167	0.1008	0.0167
$\bar{p}$	0.0479		0.0479		0.0504		0.0502	

14 and 16 degrees C were less than 2, results were ultimately not influenced by the choice of threshold.

We consequently fit integrated dynamic models for a total of 28 covariate combinations, however, eight cases resulted in some very large standard error estimates. In these latter cases, all were models where productivity varied with at least year and degree-days (for which the Pearson's correlation coefficient was approximately 0.6), and they showed a minimum eigenvalue of the Hessian that was close to zero, suggesting that not all parameters were individually estimable. This finding was replicated for alternative thresholds for the degree-days covariate. The top 10 of the 20 remaining models are shown in Table 3.

The model with lowest AIC had 23 parameters and year-varying productivity that also

Table 2: Parameter estimates (with standard errors, SE) for the dynamic model fitted to the count data alone with constant (i) and time-varying mean emergence date μ (ii); the number of parameters is denoted by n. σ represents the standard deviation of the emergence period. Annual estimates of productivity ρ, overall abundance G and time-varying μ are provided in Figure S1 of the Supporting Information.

	i)		ii)	
n	20		38	
AIC	5155.2		4972.0	
Parameter	Estimate	SE	Estimate	SE
μ	65.09	14.09	time-varying	
σ	34.75	5.83	21.93	1.72
ϕ	0.98	0.03	0.90	0.04

Table 3: Range of models fitted with covariates, with associated AIC and ΔAIC values. The formulae describe the formulation for productivity, ρ, and detection probability, p, respectively. This is a truncated table of the models with the ten smallest AIC values. Mean emergence date μ and spread of the emergence period σ were assumed to be constant in all models. n is the number of parameters estimated and D is the estimated scaled deviance. HL denotes heat load, DD indicates degree-day, DUR indicates survey duration, and TEMP is a measure of daily mean temperature in Basel.

Model	n	D	AIC	ΔAIC
$\rho \sim$YEAR+HL, $p \sim$DUR	23	1.615	5183.4	0.0
$\rho \sim$YEAR+HL, $p \sim$DUR+TEMP	24	1.614	5191.5	8.1
$\rho \sim$YEAR+HL, $p \sim$TEMP	23	1.634	5198.8	15.4
$\rho \sim$YEAR+HL, $p \sim$DUR+TEMP+I(TEMP^2)	25	1.616	5200.1	16.8
$\rho \sim$YEAR, $p \sim$DUR	22	1.627	5211.0	27.6
$\rho \sim$YEAR, $p \sim$DUR+TEMP	23	1.626	5219.1	35.7
$\rho \sim$YEAR, $p \sim$DUR+TEMP+I(TEMP^2)	24	1.628	5228.9	45.5
$\rho \sim$YEAR, $p \sim$TEMP	22	1.650	5231.1	47.7
$\rho \sim$HL+DD, $p \sim$DUR	8	1.868	5719.8	536.4
$\rho \sim$HL+DD, $p \sim$DUR+TEMP	9	1.866	5726.1	542.7

varied with site heat load, and detection varying with survey duration. Inspection of the second best model showed the addition of temperature for detection was not needed. Refitting the top model in Table 3 but with year-varying (rather than constant) mean emergence date μ greatly reduced the AIC to 4984.9, with 41 parameters. The scaled deviances of these models were 1.62 and 1.52, respectively, suggesting adequate descriptions of the data, albeit with a moderate amount of overdispersion relative to the basic Poisson model assumed. For estimates of the year-constant parameters see Table 1c) and d). Differences between parameter estimates for the models with and without the site heat load parameter were minimal (Table 1).

Productivity under model d) varied greatly between years and correlated positively with site heat load (Figure 1). Estimates of peak emergence date μ varied from about 20 to 90 (Figure 2), becoming later by roughly one month over the period studied, but also less variable. The additional site heat load parameter for productivity did not have much influence on the estimates of μ (see Figure S3 of the Supporting Information).

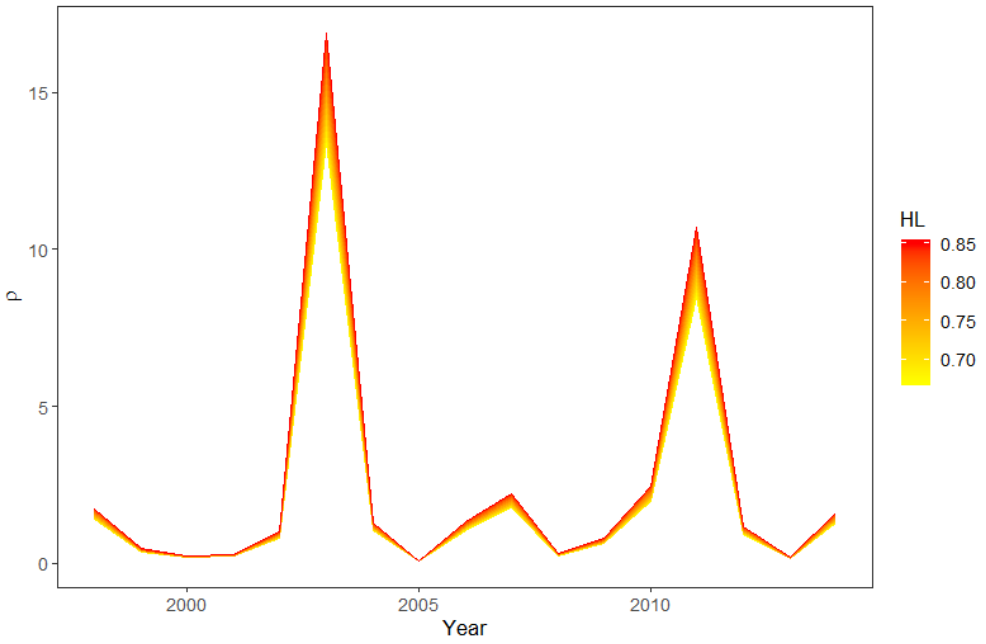

Figure 1: Estimated productivity, ρ, for each year across the range of site heat load (HL) values from the best-fitting integrated model with year-varying μ. Confidence bands are not presented, but Figure S2 of the Supporting Information presents confidence bands for the model where HL is not included.

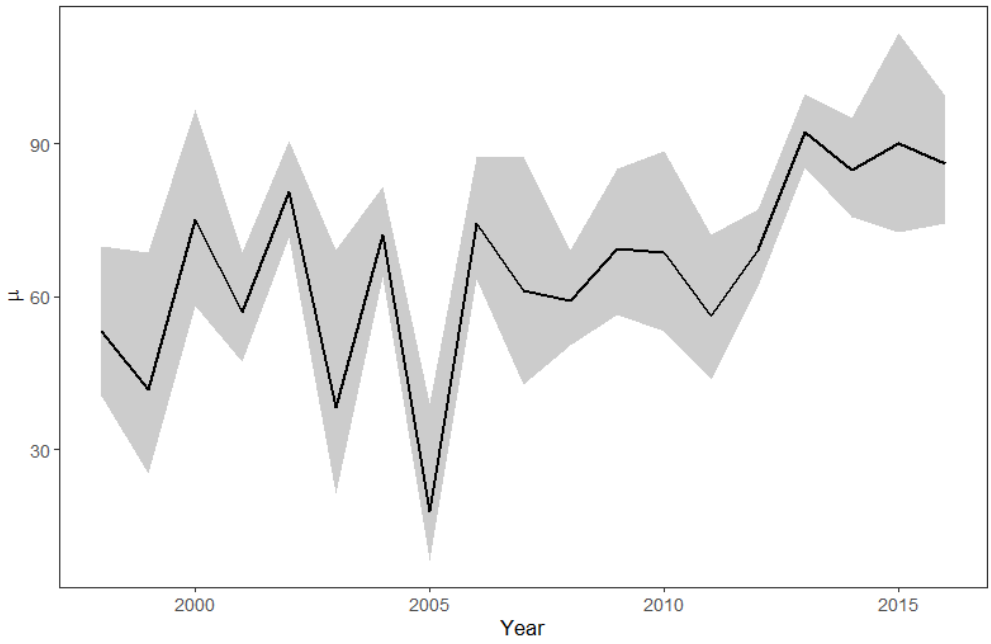

Figure 2: Estimated mean emergence date, μ, per year measured in days from the best-fitting integrated model with year-varying μ, and associated 95% confidence intervals. Day 60 corresponds to 15 April.

Estimates of absolute population size G under the best-fitting model (d in Table 1) are shown in Figure 3 and indicate a downward trend over time. Estimates of G were similar across all four IPMs fitted (see Figure S4 of the Supporting Information), although note the difference in scale relative to the model applied to count data alone, where detection probability, p, is not separated from abundance N and where the latter therefore has a 'relative abundance' interpretation only (Supporting Information Figure S1c). Low population sizes for the odd year populations increase as a consequence of increased productivity values shown in Figure 1.

3.3. Model fit

The best-fitting model had a scaled residual deviance of 1.52, suggesting moderate overdispersion relative to the Poisson assumption. We investigated this further by fitting the best model using one-step of the iterated methods necessary for concentrated likelihood for Zero-inflated Poisson (ZIP) and negative-binomial models (Dennis et al., 2016a). This was done as a check, as full fitting of these models is computer intensive. Examples considered

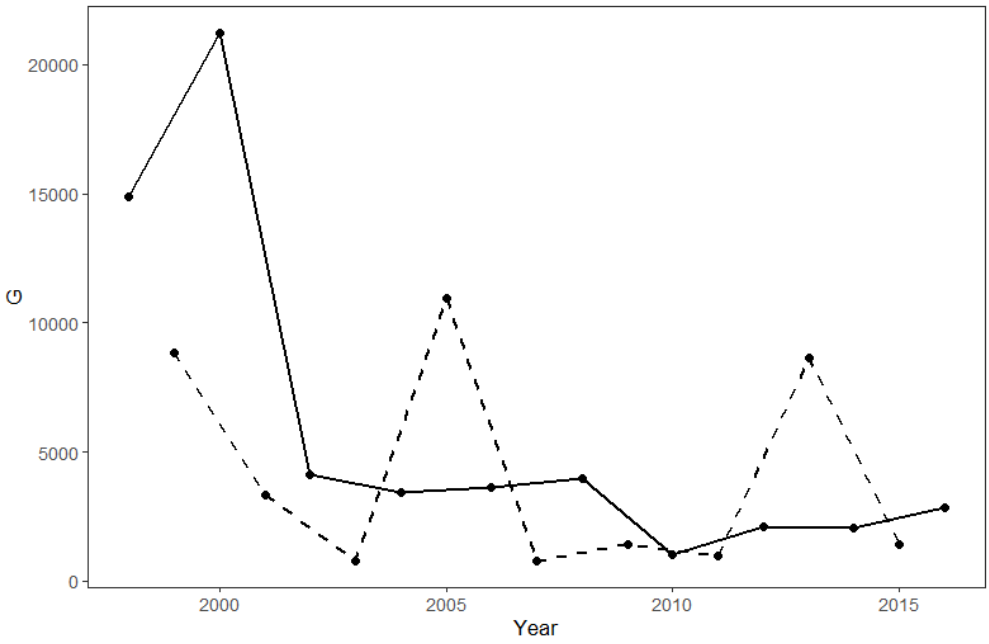

Figure 3: Estimated population size G (the total number of beetles ever alive across all sites) each year from fitting the best-fitting integrated model with year-varying μ. We distinguish between those individuals that are imagos in the first year of the study (even years, solid line) and those that become imagos one year later (odd years, dashed line). Estimated confidence bands are not given, but could be achieved with a computationally expensive bootstrap.

in Dennis et al. (2016a) suggested only a small amount of iteration was typically necessary. Here the ZIP model decreased the AIC and resulted in a reduced scaled deviance of 1.42, whereas the NB model appeared to overfit the data. Comparisons of parameter estimates between fitting the Poisson and ZIP models (Figure S5 of the Supporting Information) show that the two models yield point estimates that are identical for all practical purposes and that only the imprecision is larger under the ZIP-version of the AIC-best model. Similar results were obtained for the negative binomial, but with larger standard errors. We conclude that the Poisson fit is acceptable, and that changing the distribution does not change our conclusions. Quasi-likelihood arguments could be used to increase the standard errors by multiplying by the square root of the Poisson scaled deviance (Dennis, 2015), however the change is minimal in this case, with standard errors increased by 23%.

4. Discussion

4.1. Modelling population dynamics at two temporal scales

We believe that (temporally) multi-scale population dynamics are common. For example, many species of insects have generation times that exceed one year, e.g., some dragonflies, many large beetles and famously cicadas, for all of which the larval stage lasts for more than one year, while the imagos have life spans of the order of days to weeks. However, the only relevant models are the open-robust-design (ORD) model of Kendall and Bjorkland (2001), those of DMFRB, and a further variation on the model of DMFRB which describes data on bumblebees (Matechou et al., 2018). The ORD model is designed for a classical capture-recapture study with individually marked animals, where there are primary and secondary capture occasions, but where closure cannot be assumed among the secondary occasions within the same primary occasion. Instead, in the ORD model population gains and losses are modelled both among secondary as well as among primary occasions.

In contrast, the models developed by DMFRB can be fitted to simple counts of unmarked individuals, but they require spatial replication, i.e., multivariate time-series of counts from replicated sites/populations. While the between-season component of these models is usually rather simple (e.g., an exponential population model), several formulations are possible for the within-season dynamics, e.g., purely phenomenological approaches such as a GAM or a Gaussian curve, or more mechanistic birth/death processes such as the MZ model.

Demographic models for insects that contain explicit parameters for the underlying birth/death processes are very rare, presumably because of the difficulty with which insects can be studied by capture-recapture. The ability of the MZ-type of models, including those by DMFRB and the one in this study, to estimate such demographic parameters from simple counts of unmarked individuals, is a great advantage and should enhance the demographic modelling of many insect species which can be counted. Moreover, it may be beneficial to consider whether further information about some of the model parameters can be obtained, such as by conducting additional, but spatially and temporally restricted, capture-recapture studies. Such an integrated population model for an insect species has been formulated by

Gross et al. (2007), who augment the MZ model with information from a capture-recapture study. However they do not link the abundance parameters across years by a population model as we do.

4.2. Biology of I. fuliginator

While we made the assumptions of constancy for both the spread of emergence times (σ) and apparent survival (ϕ), we found strong evidence for annual variation of productivity (ρ) and mean emergence date (μ), as well as, consequently, total annual population size (G).

There was considerable annual variation in productivity, and 2003 and 2011 stood out in particular, as well as 2007 to a lesser degree. These were also the years with the overall smallest estimated total population sizes. Thus, there seemed to be a stabilizing tendency in the population dynamics, in that increases were most marked when population sizes were lowest. This may reflect density-dependence.

In the Basel population, the day of first emergence was related to the mean daily temperature for February and March in the years 1985–2000 (Baur et al., 2002). In this study, there was also annual variation in the estimates of mean emergence date, which spanned more than two months and seemed to show two phases: with no trend but great year-to-year fluctuations up until 2006, followed by a much smoother trajectory with an increasing trend thereafter, where mean emergence date became about one month later in the last decade. Winter temperatures appear to have increased over this period in the study area (unpublished data) and this delay in appearance may appear counter-intuitive. However, it ties in with what is known about the physiology of insects with an obligate diapause, and which typically need a certain amount of cold temperatures to break diapause (W. Blanckenhorn, pers. comm.). For instance, Stålhandske et al. (2017) found that milder winters lead to significant delays in the emergence of three out of five species studied and wrote: "the delaying effect of winter warmth has become more pronounced in the last decade, during which time winter durations have become shorter." Thus climate change may have counter-intuitive effects on phenology.

Our models confirmed a serious decline of the beetle total annual abundance over the 19

years of study. A simple linear regression of the total annual abundance (in Figure 3) on year suggested a decline by about 98% (from approximately 9900 individuals to only about 250) which is comparable with findings in Baur et al. (2020), who suggest that habitat deterioration may be responsible for the decline of this specialised species. Although the time-series of counts are statistically-speaking short, there appears to be a difference between the two annual cohorts, with a potentially stronger decline and more even trajectory for the even-year cohorts whereas, in contrast, the odd-year cohorts hardly appear to exhibit a long-term trend, but show more pronounced annual fluctuations. The biological reasons underlying this pattern are unknown, and in particular the reasons for the changes in 2005 and 2013, for example whether these may be linked to particular temperature changes.

The covariate modelling identified heat load and year as important effects for productivity, with much less evidence for degree-days, although this may have been influenced by the apparent correlation between degree-days and year. As expected, the effect of heat load was positive. For detection probability, there was a clear positive effect of survey duration, also as expected. There was limited evidence for alternative covariates given the differences in AIC for alternative models. Further work could consider the effects of suitable covariates on other stages of the life cycle of *I. fuliginator* (Suppo et al., 2020).

Under simple assumptions of constancy, longevity of imagines of *I. fuliginator* can be estimated from apparent survival (ϕ) as $1/(1-\phi)$. Under model (d) in Table 1, this yields only 8.2 days (SE = 0.6). This species of beetle is a striking example of an insect life-cycle with an extremely short adult stage compared to the earlier life-stages.

Detection probability was very low and estimated at about 0.05 per survey occasion (on average across the survey durations). This could be an underestimate if the population is not closed during the count surveys and the counts really refer to some kind of superpopulation. However, we believe this to be quite unlikely given the limited dispersal distances of the beetle (Baur et al., 2005), the duration of the sampling periods, the size and configuration of the habitat patches and also the short longevity of the beetles. Such low values emphasize the need for estimating detection probability for such insects when true population sizes are

needed, for instance, in a population viability analysis (Beissinger and Westphal, 1998).

In the Basel population, a flagship for local biodiversity conservation, the last 52 visits did not detect a single beetle. Even under the unlikely assumption that the population always consisted of exactly one surviving beetle, the aggregated probability to detect that beetle at least once (and therefore to ascertain population survival) can be estimated as $1 - (1 - p)^{52} = 0.93$. This probability increases to 0.97 if there are always exactly two independent beetles and to > 0.99 for three or more. Hence, despite the low detection probability, not observing any beetles during all these surveys strongly suggests there are none left (McArdle, 1990; Kéry, 2002) and that the Basel population is now sadly extinct.

4.3. Avenues for future research

Despite the concentrated likelihood and the multivariate normal approximation to the joint likelihood of the IPM, fitting these models is computer-intensive. We therefore made some constancy assumptions, including for the spread of the date of emergence (σ) and apparent survival (ϕ). Calabrese (2012) shows that inferences under MZ-types of models can be strongly dependent on the parametric assumptions made about entry and exit probabilities, especially about the constancy of survival. For instance, Matechou et al. (2014) discovered that a model with linear and quadratic time effects on survival was best supported by AIC, and such a structure on ϕ might also be investigated here.

We assumed a strict biennial life-cycle of *I. fuliginator* in our study area, which is in accordance with all published information and also with conventional wisdom among entomologists. Interestingly, recent genetic analyses revealed the absence of any differentiation between the cohorts from odd and even years (B. Baur, unpubl. data), which might seem to cast doubt on this important assumption, since it may suggest that individuals achieve eclosion within one, two or three years. However, findings in population genetics indicate that one reproducing migrant per generation is enough to prevent genetic differentiation between populations (Mills and Allendorf, 1996). Hence, it is quite probable that the vast majority of the beetles do adhere to a biennial life-cycle, thus making our model adequate. Nevertheless, it would be interesting to extend the modelling of this paper to allow for vari-

ation in duration of lifetime and larval polymorphism, which could have relevance for other species and taxa exhibiting this trait. The possibility of hot and dry conditions affecting the time to maturity could also be considered further.

Further research would be valuable considering the interest and attractions in adding random effects to account for spatial and temporal correlations, as well as to fit multi-species versions of the models. Multi-scale spatial models are another avenue for further research, to describe population dynamics within and between sites (Raffa et al., 2008; Wildemeersch et al., 2019).

5. Conclusions

We believe that population dynamics with more than a single temporal scale is much more common than previously recognized. Therefore, we consider the chief conceptual interest of the modelling in this paper, and that in DMFRB, to be the focus on multiple temporal scales of population dynamics. For cases such as insects or migrating animals it is immediately obvious that a model is needed which describes population dynamics at two temporal scales. In butterflies and seasonally migrating animals, the between-season dynamics will typically be that of a first-order Markov process with respect to time, while in some species with generation time longer than one year such as some beetles, dragonflies and cicadas, a longer-range dependency is needed.

However, the importance of the kind of model presented here on multi-scale population dynamics models may transcend the simple examples of insects and migrating animals. Indeed, it may represent a very general modelling framework that enables one to relax the typical closure assumption in much of traditional population dynamics modelling and may be applied to both the dynamics of reproducing populations or that of migratory animals at staging areas or other points along their journey. Hence, for instance, for breeding birds, rather than assuming a closed and constant population within what we call a breeding season, we would model the within-season dynamics of territory establishment and abandonment by territory holders in a very flexible and general way, or similarly for pond-breeding amphibians or beach-nesting sea-turtles. Finally, we could envisage beneficial combinations between the

models in this paper and DMFRB and the ORD models of Kendall and Bjorkland (2001). Such potential hybrid models would again fall under the rubric of integrated population models and provide powerful tools for improved inferences in population dynamics.

6. Acknowledgements

Wolf Blanckenhorn made valuable comments on insect physiology. We thank two anonymous reviewers for their comments and Takis Besbeas for using hidden Markov models to check the deterministic approximation of the dynamic models. We thank all colleagues who have contributed to the beetle surveys over the years and Samuel Zschokke for compiling the soil temperature data. Beetle monitoring has received financial support from the Stadtgärtnerei Basel. Financial support of this study was provided by a grant from the Swiss National Science Foundation (No 31003*A*.1464125 to M. Kéry and M. Schaub). BJTM was supported by a Leverhulme Emeritus fellowship.

References

Baur, B., Burckhardt, D., Coray, A., Erhardt, A., Heinertz, R., Ritter, M., Zemp, M., 1997. Der Erdbockkäfer, *Dorcadion fuliginator* (L., 1758)(Coleoptera:Cerambycidae), in Basel. Mitteilungen der Entomologischen Gesellschaft Basel 47, 59–124.

Baur, B., Coray, A., Lenzin, H., Schmera, D., 2020. Factors contributing to the decline of an endangered flightless longhorn beetle: A 20-year study. Insect Conservation and Diversity 13, 175–186.

Baur, B., Coray, A., Minoretti, N., Zschokke, S., 2005. Dispersal of the endangered flightless beetle *Dorcadion fuliginator* (Coleoptera: Cerambycidae) in spatially realistic landscapes. Biological Conservation 124, 49–61.

Baur, B., Zschokke, S., Coray, A., Schläpfer, M., Erhardt, A., 2002. Habitat characteristics of the endangered flightless beetle *Dorcadion fuliginator* (Coleoptera: Cerambycidae): implications for conservation. Biological Conservation 105, 133–142.

551 Beissinger, S.R., Westphal, M.I., 1998. On the use of demographic models of population
552 viability in endangered species management. The Journal of Wildlife Management 62,
553 821–841.

554 Besbeas, P., Freeman, S.N., Morgan, B.J.T., Catchpole, E.A., 2002. Integrating mark–
555 recapture–recovery and census data to estimate animal abundance and demographic pa-
556 rameters. Biometrics 58, 540–547.

557 Besbeas, P., Lebreton, J.D., Morgan, B.J.T., 2003. The efficient integration of abundance and
558 demographic data. Journal of the Royal Statistical Society: Series C (Applied Statistics)
559 52, 95–102.

560 Besbeas, P., Morgan, B.J., 2020. A general framework for modeling population abundance
561 data. Biometrics 76, 281–292.

562 Besbeas, P., Morgan, B.J.T., 2019. Exact inference for integrated population modelling.
563 Biometrics 75, 475–484.

564 Böhning, D., van der Heijden, P.G., Bunge, J., 2017. Capture-recapture Methods for the
565 Social and Medical Sciences. CRC Press.

566 Buckland, S.T., Rexstad, E.A., Marques, T.A., Oedekoven, C.S., 2015. Distance sampling:
567 methods and applications. Springer, Cham, Switzerland.

568 Calabrese, J.M., 2012. How emergence and death assumptions affect count-based estimates
569 of butterfly abundance and lifespan. Population Ecology 54, 431–442.

570 Caswell, H., 2001. Matrix population models. Oxford University Press.

571 Dennis, E., 2015. Development of statistical methods for monitoring insect abundance. Ph.D.
572 thesis. University of Kent.

573 Dennis, E.B., Morgan, B.J.T., Freeman, S.N., Brereton, T.M., Roy, D.B., 2016a. A general-
574 ized abundance index for seasonal invertebrates. Biometrics 72, 1305–1314.

575 Dennis, E.B., Morgan, B.J.T., Freeman, S.N., Roy, D.B., Brereton, T., 2016b. Dynamic
576 models for longitudinal butterfly data. Journal of Agricultural, Biological and Environ-
577 mental Statistics 21, 1–21.

578 Gross, K., Kalendra, E.J., Hudgens, B.R., Haddad, N.M., 2007. Robustness and uncertainty
579 in estimates of butterfly abundance from transect counts. Population Ecology 49, 191–200.

580 Kendall, W.L., Bjorkland, R., 2001. Using open robust design models to estimate temporary
581 emigration from capture-recapture data. Biometrics 57, 1113–1122.

582 Kéry, M., 2002. Inferring the absence of a species: a case study of snakes. The Journal of
583 Wildlife Management 66, 330–338.

584 Koons, D.N., Arnold, T.W., Schaub, M., 2017. Understanding the demographic drivers of
585 realized population growth rates. Ecological Applications 27, 2102–2115.

586 Laake, J.L., Johnson, D.S., Conn, P.B., 2013. marked: An R package for maximum-likelihood
587 and MCMC analysis of capture-recapture data. Methods in Ecology and Evolution 4, 885–
588 890.

589 Manly, B.F.J., 1974. Estimation of stage-specific survival rates and other parameters for
590 insect populations developing through several stages. Oecologia 15, 277–285.

591 Matechou, E., Dennis, E.B., Freeman, S.N., Brereton, T., 2014. Monitoring abundance and
592 phenology in (multivoltine) butterfly species: a novel mixture model. Journal of Applied
593 Ecology 51, 766–775.

594 Matechou, E., Freeman, S.N., Comont, R., 2018. Caste-specific demography and phenology
595 in bumblebees: modelling *bee walk* data. JABES 23, 427–445.

596 Matechou, E., McCrea, R.S., Morgan, B.J.T., Nash, D.J., Griffiths, R.A., 2016. Open models
597 for removal data. The Annals of Applied Statistics 10, 1572–1589.

Matechou, E., Morgan, B.J.T., Pledger, S., Collazo, J., Lyons, J., 2013. Integrated analysis of capture–recapture–resighting data and counts of unmarked birds at stop-over sites. Journal of Agricultural, Biological, and Environmental Statistics 18, 120–135.

McArdle, B.H., 1990. When are rare species not there? Oikos 57, 276–277.

McCrea, R.S., Morgan, B.J.T., 2014. Analysis of capture-recapture data. Chapman and Hall/CRC.

McCune, B., Keon, D., 2002. Equations for potential annual direct incident radiation and heat load. Journal of Vegetation Science 13, 603–606.

Mills, L.S., Allendorf, F.W., 1996. The one-migrant-per-generation rule in conservation and management. Conservation Biology 10, 1509–1518.

Morgan, B.J.T., 2009. Applied Stochastic Modelling. Texts in Statistical Science. 2nd ed., CRC Chapman & Hall.

R Core Team, 2018. `R`: A Language and Environment for Statistical Computing. Technical Report. Vienna, Austria. `http://www.R-project.org/`.

Raffa, K.F., Aukema, B.H., Bentz, B.J., Carroll, A.L., Hicke, J.A., Turner, M.G., Romme, W.H., 2008. Cross-scale drivers of natural disturbances prone to anthropogenic amplification: the dynamics of bark beetle eruptions. Bioscience 58, 501–517.

Schaub, M., Abadi, F., 2011. Integrated population models: a novel analysis framework for deeper insights into population dynamics. Journal of Ornithology 152, 227–237.

Schaub, M., Kéry, M., 2021. Integrated Population Models. Academic Press.

Schaub, M., Pradel, R., Jenni, L., Lebreton, J.D., 2001. Migrating birds stop over longer than usually thought: an improved capture–recapture analysis. Ecology 82, 852–859.

Stålhandske, S., Gotthard, K., Leimar, O., 2017. Winter chilling speeds spring development of temperate butterflies. Journal of Animal Ecology 86, 718–729.

622 Suppo, C., Bras, A., Robinet, C., 2020. A temperature-and photoperiod-driven model reveals
623 complex temporal population dynamics of the invasive box tree moth in Europe. Ecological
624 Modelling 432, 109229.

625 Wildemeersch, M., Franklin, O., Seidl, R., Rogelj, J., Moorthy, I., Thurner, S., 2019. Mod-
626 elling the multi-scaled nature of pest outbreaks. Ecological Modelling 409, 108745.

627 Zonneveld, C., 1991. Estimating death rates from transect counts. Ecological Entomology
628 16, 115–121.